Acta Crystallographica Section B
Structural Science
ISSN 0108-7681

Modulated structure and phase transitions of $Sr_{10}Ga_6O_{19}$

Hannes Krüger,[a]* Biljana Lazić,[b] Erik Arroyabe[a] and Volker Kahlenberg[a]

[a]Institute of Mineralogy and Petrography, University of Innsbruck Austria, and [b]Institute of Geology, University of Bern, Switzerland

Correspondence e-mail: hannes.krueger@gmail.com

Received 16 June 2009
Accepted 9 July 2009

The crystal structure of $Sr_{10}Ga_6O_{19}$ was investigated by *in situ* single-crystal X-ray diffraction in the temperature range 298–673 K. At ambient conditions the compound shows a (3 + 1)-dimensional modulated structure in the superspace group $C2/c(0\beta0)s0$ [a = 34.9145 (13), b = 7.9369 (2), c = 15.9150 (7) Å and β = 103.551 (3)°] with a modulation wavevector of $\mathbf{q}$ = 0.4288 (2)$\mathbf{b}$*. Whereas the presented structural model uses first-order harmonic modulation functions only, some features of the modulations are discussed utilizing an electron density derived by the maximum entropy method. Furthermore, two phase transitions were identified: between 453 and 503 K the incommensurate superstructure is replaced by a doubling of the a and b lattice constants, and between 503 and 673 K a phase with the basic cell is formed, identical to α-$Sr_{10}Ga_6O_{19}$. Under some cooling conditions crystals showing a combined diffraction pattern of both superstructures can be obtained. The relation of these results to α-$Sr_{10}Ga_6O_{19}$ [Kahlenberg (2001). *J. Solid State Chem.* **160**, 421–429] is discussed.

1. Introduction

In previous years the phase relationships in the binary system SrO–Ga_2O_3 have been re-investigated in more detail (Zinkevich, 2007). This interest can be at least partially attributed to the fact that alkaline earth gallates are potential host materials for the production of luminescent compounds (Poort *et al.*, 1995; Yang & Tu, 2005). Especially in the more SrO-rich part of the system the thermodynamic assessment has been aided by several structural characterizations proving or disproving the existence of phases whose existence has been postulated in previous studies (Kahlenberg, 2001, 2002; Kahlenberg *et al.*, 2005). Owing to the combination of large unit-cell volumes, low overall space-group symmetries and pronounced pseudo-symmetries of the cation substructures, the structure determinations were not straightforward and frequently resulted in crystallographically challenging problems. In the course of these investigations it became obvious that $Sr_{10}Ga_6O_{19}$ occurs in two similar but distinct modifications: a monoclinic α as well as an orthorhombic β phase. Both compounds are based on non-cyclic tetrahedral [Ga_6O_{19}] units. From a structural point of view the two polymorphs differ with respect to the conformation of these groups as well as their packing. However, the stability ranges of both forms are still not known. In the course of a study primarily aimed to settle this question we obtained single crystals of a previously unknown incommensurately modulated polymorph. The present manuscript reports a detailed structural description of this new phase and its high-temperature behaviour.

Table 1
Crystal data and experimental details.

	298 K	673 K
Crystal data		
Chemical formula	$Sr_{10}Ga_6O_{19}$	$Sr_{10}Ga_6O_{19}$
M_r	1598.5	1598.5
Crystal system, (super)space group	Monoclinic, $C2/c(0\beta0)s0$	Monoclinic, $C2/c$
a, b, c (Å)	34.9145 (13), 7.9369 (2), 15.9150 (7)	35.0481 (18), 7.9732 (4), 16.0077 (8)
β (°)	103.551 (3)	103.492 (4)
Modulation wavevector (**q**)	0.4288 (2)**b***	–
V (Å^3)	4287.5 (3)	4349.8 (4)
Z	8	8
D_x (Mg m^{-3})	4.95	4.88
Radiation type	Mo $K\alpha$	Mo $K\alpha$
μ (mm^{-1})	32.1	31.67
No. of reflections for cell parameters	21 142	6600
Crystal form, size (mm)	Fragment, 0.2 × 0.14 × 0.1	Fragment, 0.2 × 0.14 × 0.1
Data collection		
Diffractometer	Stoe IPDS-II	Stoe IPDS-II
Data collection method	Rotation method	Rotation method
No. of frames measured	720/360	360
Range in ω; increment (°)	0–180; 0.25/0.5	0–180; 0.5
Exposure time (min)	16/0.5	10
Absorption correction	Gaussian	Gaussian
T_{max}, T_{min}	0.188, 0.065	0.183, 0.081
Reflection ranges	$-42 \le h \le 42$	$-42 \le h \le 42$
	$-9 \le k \le 9$	$-9 \le k \le 9$
	$-19 \le l \le 18$	$-19 \le l \le 19$
	$-1 \le m \le 1$	–
No. of measured reflections	47 585	14 385
Reflections used in refinement (main; sat.)	7637; 7942	3902; –
Observed reflections used in refinement (main; sat.)	4572; 5961	3173; –
Criterion for observed reflections	$I > 3\sigma(I)$	$I > 3\sigma(I)$
R_{int}	0.071	0.082
θ_{max} (°)	25.9	25.7
Refinement		
Refinement on	F	F
R_{obs} (all; main; sat.)	0.084; 0.053; 0.136	–; 0.055; –
wR_{all} (all; main; sat.)	0.073; 0.051; 0.113	–; 0.051; –
S (all)	2.65	2.47
Weighting scheme	$w = 1/[\sigma^2(F) + (0.01F)^2]$ based on σ	$w = 1/[\sigma^2(F) + (0.01F)^2]$ based on σ
No. of parameters	947	318
$(\Delta/\sigma)_{max}$	0.001	< 0.0001
$\Delta\rho_{max}$, $\Delta\rho_{min}$ (e Å^{-3})	5.43, −4.45	1.67, −1.77
Extinction method	Isotropic, type 1, Gaussian (Becker & Coppens, 1974)	Isotropic, type 1, Gaussian (Becker & Coppens, 1974)
Extinction coefficient	2036 (110)	5086.46

2. Experimental

2.1. Synthesis

Dried $SrCO_3$ (AlfaAesar, puratronic) as well as Ga_2O_3 (Riedel de Haën, puriss) were used as educts for the single-crystal growth experiment. A stoichiometric mixture giving 1 g of $Sr_{10}Ga_6O_{19}$ was carefully homogenized in an agate mortar under ethanol, transferred into a platinum crucible and then heated within 20 h from 773 to 1773 K. The sample was held at this temperature for 6 h before being cooled to 1473 K at a rate of 10 K h^{-1}. Subsequently, the controller was adjusted to a setpoint of 473 K and the heating power was switched off. The furnace cooled to 473 K according to an exponential function: 973 K was reached 40 min later, after 90 min the temperature was 673 K and finally after *ca* 270 min the setpoint of 473 K was reached. After *ca* 5 h at this temperature the sample was removed from the furnace. A first check of the run-product *via* polarization microscopy revealed the existence of crystals of good optical quality embedded in a small amount of glass. A more detailed investigation by powder X-ray diffraction (XRD) revealed that no significant amounts of any other phase could be detected.

2.2. X-ray diffraction

The single-crystal X-ray diffraction experiment at ambient temperature revealed a *C*-centred monoclinic cell with lattice constants as given in Table 1. Their values are in good agreement with those previously reported for this compound (Kahlenberg, 2001). Furthermore, weak satellite reflections were observed. They can be indexed with a vector **q** = 0.4288 (2)**b***.

In order to obtain suitable intensities for the weak satellite reflections, the data collection was performed using ω increments of 0.25° with 16 min of exposure for each frame. Since many (*ca* 140) strong reflections were overexposed, a second run was carried out, utilizing 0.5° ω rotations with 30 s of irradiation. The two data-collection runs were integrated independently and corrections for Lorentz and polarization effects, as well as for air and sample absorption (using 14 indexed crystal faces), were applied. During the optimization of the profile parameters a large weighting factor for avoiding overlap conditions was used (Stoe & Cie GmbH, 2007). The data integration was performed with a 5% overlap tolerance. However, approximately 14% of the reflections were rejected because of overlapping of the profiles.

Fig. 1(*a*) shows the *hk*1 layer of the reciprocal space, reconstructed from the data collection described above. The overlaid reciprocal lattice accounts for the *C*-centred basic cell only, the reflections not coinciding with the lattice nodes are the incommensurate satellites. Only the first-order satellites exhibit intensities high enough to be measured. In the original reciprocal space images, second-order satellites can be seen

occasionally, although on average their intensities are far too weak to be useful for the refinement. From the point of intensities, this experiment is at the limits of ordinary laboratory equipment (9 d of data collection). Further improvement could be obtained with a rotating anode or synchrotron radiation.

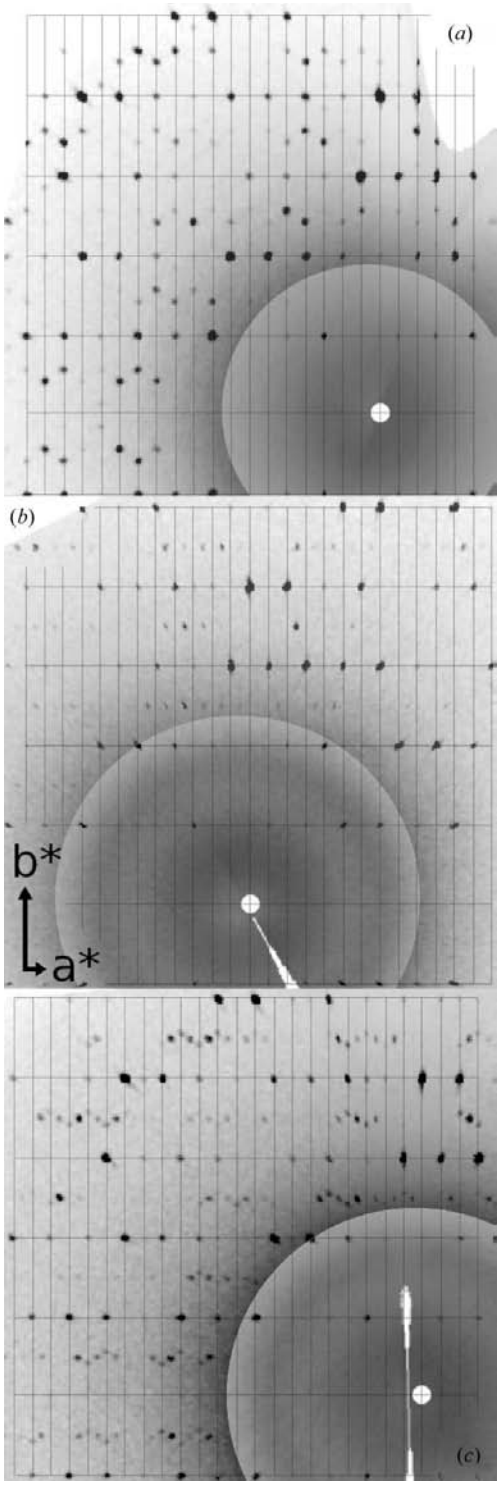

Figure 1
Reconstructed reciprocal space layers *hk*1. (*a*) Initial data collection at ambient temperature, (*b*) high-temperature measurement at 503 K and (*c*) another ambient condition experiment after the high-temperature treatment. The big white spot marks the origin (001) of the layer. See text for further details.

The data collection run with the long exposure time gave 3971 main reflections, 92% of them observed, their average $I/\sigma(I)$ is 62. Furthermore, 7942 satellites of first order with an average $I/\sigma(I)$ of *ca* 11 (75% observed) were measured. 50% of the satellites are below $I/\sigma(I) = 5.5$. However, as shown here, the data is good enough to reveal the basic features of the modulations.

Analysis of the diffraction pattern revealed the extinction symbol *C*1*c*1, which is in agreement with the space group $C2/c$ (Kahlenberg, 2001). Furthermore, none of the (0*k*0*m*) reflections with $m = 1$ is observed, which points to the superspace group $C2/c(0\beta0)s0$ [No. 15.3, listed as $B2/b(00\gamma)s0$ in the *International Tables for Crystallography* (Janssen *et al.*, 2004)].

2.3. High-temperature X-ray diffraction

High-temperature experiments were performed on the Stoe IPDS II diffractometer using the Stoe Heatstream device. Setup of the experiment and calibration of the temperature was carried out as described by Krüger & Breil (2009). The same crystal as used for the data collection at ambient temperature was fixed in a tight-fitting (0.1 mm) capillary made from fused SiO_2.

To evaluate possible changes of the modulation or the structure, five data collections at elevated temperatures were carried out. The measurement conditions were chosen to account for the weak satellite reflections: 10 min exposure time for each 0.5° step of ω rotation. Experiments at 363, 383, 413 and 453 K still show the existence of the satellite reflections with $\mathbf{q} = 0.429\mathbf{b}*$. A significant change of **q** could not be detected. The fifth experiment at *ca* 503 K revealed a change in the diffraction pattern: the incommensurate satellite reflections had disappeared, but new commensurate superstructure reflections emerged at positions which double the *a* and *b* lattice constants [a = 70.005 (4), b = 15.901 (1), c = 15.982 (1) Å, β = 103.618 (1)°]. Fig. 1(*b*) shows the *hk*1 layer reconstructed from the 503 K data collection. To point out the new superlattice reflections, the basic lattice of the structure at ambient temperature is shown. New weak reflections emerged at positions between the lattice nodes. Furthermore, new reflections appeared on positions forbidden by the *C*-centring of the basic cell. However, the new lattice is also *C*-centred, exhibiting the extinction symbol *C*1*c*1.

After the data collection at 503 K the Heatstream furnace was ramped down to ambient temperature with a ramp of *ca* 9 K min^{-1}, controlled by *htcontrol* (Krüger & Breil, 2009).

A second ambient-temperature data collection after the high-temperature measurement (performed with 0.5° steps of ω rotation with 10 min exposure time per frame) was carried out, in order to check for reversibility of the observed transition. The *hk*1 layer obtained from the reciprocal space reconstruction is shown in Fig. 1(*c*). Basically it shows a combination of the features of the first ambient condition data

collection (satellite reflections at $\mathbf{q} = 0.429\mathbf{b}*$) and the doubling of a and b, as observed at 503 K.

In order to investigate the influence of the preceding temperature treatment on the ambient-condition diffraction pattern, a series of experiments were performed. The basic findings are: to 'reset' the diffraction pattern from Fig. 1(*c*) to Fig. 1(*a*), a preceding heating to 673 K has to be performed. Quenching or cooling with 9 K min^{-1} from 673 K to ambient conditions had the same effect. To obtain the combined diffraction pattern as in Fig. 1(*c*), the crystal had to be kept at 503 K for a longer time (*e.g.* overnight) followed by quenching or cooling with 9 K min^{-1} to ambient conditions.

As the 673 K treatment erased the high-temperature structure artifacts, we performed an *in situ* data collection at 673 K, utilizing long exposure times (10 min per ω rotation of 0.5°). The diffraction pattern clearly shows no signs of any superstructures – just the basic cell as presented by Kahlenberg (2001). A structural refinement was carried out, from which the results will be discussed below.

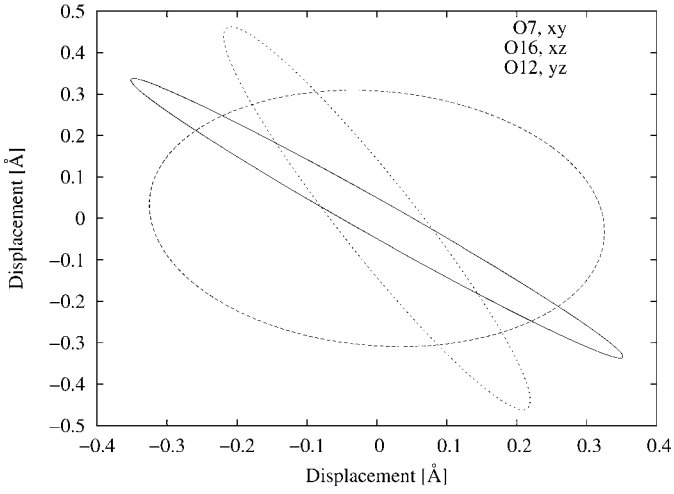

Figure 2
Displacements of the bridging oxygen atoms O7, O12 and O16 projected onto a plane. The plane (*ab*, *bc* or *bc*) is chosen to be almost perpendicular to the connection between the involved tetrahedra.

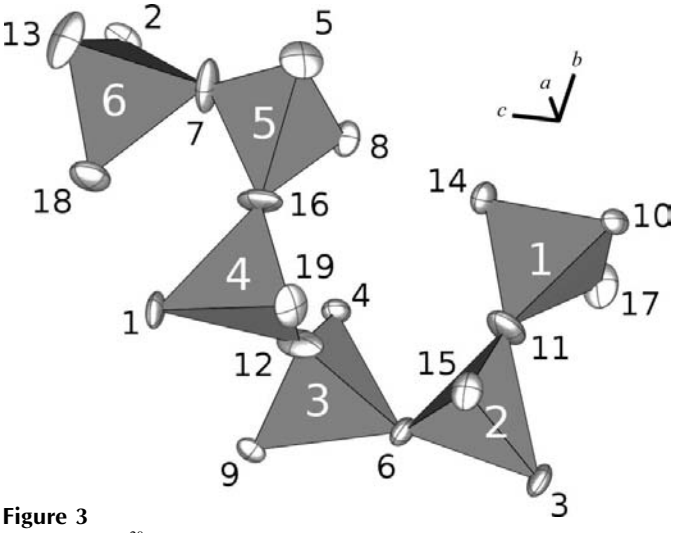

Figure 3
The $[Ga_6O_{19}]^{20-}$ hexagallate group at 673 K. The white labels give the number of the Ga atom inside the tetrahedra shown. The black labels are the numbers of the O atoms. Ellipsoids are drawn to contain 50% of the electron density (Finger *et al.*, 2007).

3. Results

3.1. Structural models

3.1.1. Modulated structure at ambient conditions. As a starting point for the analysis of the modulated structure, the structural model reported by Kahlenberg (2001) was refined using the new data. The refinement calculations were carried out using the software *JANA*2000 (Petříček *et al.*, 2000). The two datasets were used with two independent scaling factors.

The obtained fit was worse ($R_{obs} = 0.074$) than that reported before (Kahlenberg, 2001), even with a higher limit [$I/\sigma(I) = 3$] for the calculation of R_{obs}. In general, the obtained model (averaged structure) shows larger displacement parameters for the O atoms. The largest values for the equivalent isotropic displacement parameters were observed for the following atoms: O7 [0.07 (2)], O11 [0.07 (2)], O12 [0.08 (2)], O13 [0.14 (5)], O16 [0.07 (2)] and O18 [0.10 (3) Å^2]. As expected, these atoms are those showing the largest displacement caused by the modulation.

Subsequently, the structural model was expanded to the superspace group $C2/c(0\beta0)s0$ (the non-standard setting was used to retain the cell setting of Kahlenberg, 2001). For the refinement calculations of the superspace model, all reflections of the long-exposed run were used, but only the main reflections of the second faster data collection run (as the satellites of that run were far below observability). During the refinement of the modulated structure, harmonic functions of first order were employed for all atomic positions. The modulation functions for all atoms were refined independently without using constraints. Subsequently, modulation functions were introduced for the anisotropic displacement parameters.

The R_{obs} values are quite sensitive to the weak data, *e.g.* changing the observation limit from 3 to 4 $I/\sigma(I)$ decreases the R_{obs} values to 0.0680, 0.0447 and 0.1091 for all, main and satellite reflections, respectively. The values given in Table 1 were calculated using the $3I/\sigma(I)$ limit.

The largest amplitudes in the positional modulation functions can be found in the O atoms. Maxima reach 0.6 Å (y of O13, x of O18). Many O atoms show displacement up to 0.3–0.4 Å (O1, O5, O7, O11, O12, O16, O17 and O15). All the others show maximum shifts of *ca* 0.2 Å, the least modulated oxygen is O6 with maximum displacements of less than 0.1 Å. Graphs for all positional modulation functions of all atoms can be found in the supplementary material.[1] By analysing the modulation functions of the bridging oxygen atoms O7, O16 and O12 by their displacements along a, b and c (see supplementary material) the following conclusions can be made: as a function of t, O7 shows a back and forth movement in the ab plane, O16 shows a rotation about an axis more or

[1] Supplementary data for this paper are available from the IUCr electronic archives (Reference: SN5086). Services for accessing these data are described at the back of the journal.

Table 2
Bond-valence sums of $Sr_{10}Ga_6O_{19}$.

Values for the modulated structure (basic and average), as well as for the structure at 673 K.

Atom	α-$Sr_{10}Ga_6O_{19}$ (Kahlenberg, 2001)	Basic	Average	673 K
Ga1	3.17	3.08 (3)	3.00 (5)	3.06 (4)
Ga2	3.09	3.11 (3)	3.02 (5)	3.04 (4)
Ga3	2.99	2.97 (2)	2.90 (4)	2.96 (4)
Ga4	3.07	3.15 (3)	2.95 (5)	3.02 (4)
Ga5	3.23	3.27 (3)	3.09 (5)	3.17 (5)
Ga6	3.05	3.44 (3)	3.16 (6)	3.14 (4)
Sr1	1.63	1.599 (11)	1.61 (2)	1.497 (16)
Sr2	1.84	1.860 (15)	1.83 (3)	1.79 (2)
Sr3	2.39	2.445 (15)	2.40 (3)	2.38 (2)
Sr4	1.54	1.415 (11)	1.50 (2)	1.302 (16)
Sr5	2.40	2.394 (19)	2.27 (3)	2.37 (3)
Sr6	1.53	1.232 (11)	1.44 (2)	1.272 (17)
Sr7	1.25	1.222 (13)	1.43 (3)	1.223 (16)
Sr8	1.90	1.699 (16)	1.71 (3)	1.56 (2)
Sr9	1.76	1.766 (14)	1.82 (3)	1.67 (2)
Sr10	1.69	1.495 (12)	1.53 (2)	1.515 (19)
Sr11	1.73	1.464 (17)	1.66 (3)	1.39 (2)

less parallel to *b* and O12 librates in the *bc* plane. From the modulation functions of O16 (see supplementary material) a phase shift of almost $\pi/2$ can be determined between the displacements along *a* and *c*. Since the amplitudes of the displacements are nearly equal, O16 moves along an almost circular path in the *ac* plane (see Fig. 2).

In order to identify the O atoms Fig. 3 can be utilized, as it shows the $[Ga_6O_{19}]$ hexagallate unit with atom labels.

To show the modulation of the gallate group, we prepared a movie (see supplementary material), using *DRAWxtl* (Finger *et al.*, 2007), *POV-Ray* and *MEncoder*, showing the modulation of one hexagallate unit in the *t* range from 0 to 1. This movie (displayed as a loop) illustrates the above discussed structural variations in a very graphic way. The large displacements of the bridging oxygen atoms O7, O11, O12 and O16 can be seen particularly clearly. The Q^1 tetrahedron around Ga6 shows a noticeable movement involving O13 and O18. However, it can be seen that the modulation of all O atoms are correlated to such an extent that the associated tetrahedra move in a meaningful way, with regard to their connectivity.

Comparing the Ga bond-valence sums (Brown & Altermatt, 1985) of the basic structure (model of the modulated structure, but modulation functions disregarded) to the average values obtained from the modulated structure shows that the modulation relaxes the bond-valence sum (BVS) towards the expected values (with an exception for Ga3, see Table 2). This effect can also be seen for the strontium atoms (except Sr2).

Inaccuracies of the structural model can be identified from the displacement parameters. The modulated equivalent isotropic U_{eq} of some atoms show unusual values (*t* plots for all atoms are located in the supplementary material). O7 shows values varying between 0.06 and 0.005. Sr8, O5 and O18 show maxima of > 0.06 and O13 even > 0.1. Those values, of course, lack any physical meaning as they are artifacts resulting from imperfect fitting of the atomic positions by the displacive modulation functions. As the experimental evidence suggests, higher-order modulation functions are present in the structure, although higher-order satellite reflections are too weak to be measured.

To understand these features we analysed the modulations in more detail. The maximal displacement of O13 occurs along *b*. The *x*2–*x*4 F_{obs} electron density derived from a F_{obs}-Fourier synthesis (see supplementary material) shows two distinct maxima, suggesting that a crenel function is more appropriate to model the displacement function. The strong modulations on the displacement factors are easy to understand, as the atomic domain passes through low-density regions, between the crenel-like maxima. However, to obtain a clearer view on the modulations, we employed the maximum entropy method (MEM) to reconstruct the electron density from the phased structure factors. As the MEM does not depend on a structural model, it is not susceptible to model-introduced bias and especially useful to reconstruct and interpret modulation functions of incommensurate phases (Palatinus & van Smaalen, 2002, 2004; van Smaalen *et al.*, 2003). The *BayMEM* software (van Smaalen *et al.*, 2003) was used, utilizing the Sakata–Sato algorithm (Sakata & Sato, 1990). Furthermore, a flat prior was used and an *F* constraint on the fourth-order moment (Palatinus & van Smaalen, 2002, 2004). The algorithm converged after *ca* 10^5 cycles. The electron-density sections of interest were extracted with the help of the *editm*81 tool (Palatinus, 2009). The supplementary material contains a complete set of *x*1–*x*4, *x*2–*x*4 and *x*3–*x*4 electron density sections from F_{obs} as well as from the MEM. For some atoms, the refined modulation functions show a better fit to the electron density derived from the MEM, in contrast to the F_{obs} electron densities (compare O1–O5, O7, O10–O12, O15–O17, O19 and Ga5).

For many atoms it is obvious that the modulations are more complicated than the first-order harmonic functions used, which only give a good approximation. The oxygen atoms O7, O10, O11 and O13 seem to have sawtooth-like modulation functions, or combined sawtooth and harmonic displacements. Furthermore, the modulations of O4, O14, O17 and O19 show at least a partially sawtooth-like behaviour. The atoms O5, O12, O15, O18, Sr8 and Sr9 have almost separated maxima of the electron density, which is an indication of the crenel-like modulation functions.

In the end, we report the structural model as-is with first-order harmonic functions only, because all attempts to introduce sawtooth or crenel functions into the structural model failed to show better *R* values. Respecting the data quality and the parameter-to-data ratio, we refrained from trying combined modulation functions. However, the presented structural model can be useful as an approximation or as a starting point for further improvement using better data. To reveal more details of the modulation functions, a sophisticated synchrotron radiation experiment needs to deliver higher intensities of the satellite reflections, including higher-order satellites.

3.1.2. Phase at 503 K. Using the given experimental conditions, *ca* 2.1×10^4 superstructure reflections

($h \neq 2n$, $k \neq 2n$, superstructure cell) were measured, *ca* 23% of them above the $3I/\sigma(I)$ limit. The average $I/\sigma(I)$ is 2.25, which makes a meaningful analysis of the superstructure doubtful. A structural investigation of this new superstructure is reserved for synchrotron experiments. However, from our experimental evidence we can conclude that the phase transition occurs between 453 and 503 K.

3.1.3. High-temperature phase at 673 K. The data collected at 673 K was used for a structural refinement, starting from the known model of α-$Sr_{10}Ga_6O_{19}$. Details of the data collection and refinement are given in Table 1. The bond-valence sums for Ga and Sr atoms show an interesting feature compared with those of the modulated phase and α-$Sr_{10}Ga_6O_{19}$ at ambient temperature. Whereas the BVS for the Ga atoms are in good agreement, those for the Sr atoms show significantly smaller values. We interpret this as an effect of the temperature. Since the bond-valence parameters (Brown & Altermatt, 1985) were determined for structures at ambient conditions, it can be expected that structures at higher temperatures show smaller BVS. This is in fact observable for the Sr atoms, the four-coordinated gallium is less affected by thermal expansion due to the stronger bonding.

4. Discussion

From these results it is not yet clear whether the modulated $Sr_{10}Ga_6O_{19}$ phase corresponds to the α-$Sr_{10}Ga_6O_{19}$ phase (Kahlenberg, 2001). In the work of Kahlenberg (2001) satellite reflections were not observed. However, this could be a result of the experimental conditions (1.5 min exposure time per 1° rotation), which are not suitable to observe the very weak satellite reflections. At least in the product of the synthesis experiment described above, we could not find any crystals not showing satellites in their diffraction patterns. Possibly the formation of the modulated phase depends on the synthesis conditions, which were different in the earlier study. The following points may be indications that the modulated phase is different from α-$Sr_{10}Ga_6O_{19}$:

(i) the results of the refinement (Kahlenberg, 2001) show a better fit [even with a faster measurement and a lower $I/\sigma(I)$ limit for the R_{obs} values];

(ii) some anisotropic displacement parameters we obtained in the average structure are much larger than the results published earlier (Kahlenberg, 2001).

The nature of the crystal, showing the combined diffraction pattern (as in Fig. 1*c*) at ambient conditions, is still unresolved. We suggest two different explanations:

(i) it is another new phase, or

(ii) the crystal consists of coexisting domains of the high-temperature structure (doubled *a* and *b* lattice parameters) and the modulated phase.

Sophisticated diffraction experiments at a synchrotron have to be performed to reveal this. Data collections will have to deal with very weak intensities and the fact that the spacing between the satellites and the superstructure reflections corresponds to a real space lattice constant of *ca* 60 Å. Furthermore, *in situ* high-temperature experiments need to be performed at many different temperatures to elucidate the phase transition or changes in the phase ratio. The complementary technique of *in situ* transmission electron microscopy could be helpful for this future task.

5. Conclusions

The early phase-diagram studies of the system SrO–Ga_2O_3 (Batti & Sloccari, 1969; Kobzareva *et al.*, 1976) do not show a phase of the composition $Sr_{10}Ga_6O_{19}$. The diagram published by Kobzareva *et al.* (1976) contains three phases which are close to $Sr_{10}Ga_6O_{19}$: they are listed as (I) $Sr_4Ga_2O_7$ (20 mol % Ga_2O_3), (II) $Sr_7Ga_4O_{13}$ (22.2 mol % Ga_2O_3) and (III) $Sr_3Ga_2O_6$ (25 mol % Ga_2O_3). The structures of (I) and (III) have been resolved (Kahlenberg, 2001; Kahlenberg *et al.*, 2005). As already mentioned by Kobzareva *et al.* (1976) the structures show a perovskite-related subcell. Phase II has not been determined yet, which leaves room for speculation as to whether it exists at all. The composition of $Sr_{10}Ga_6O_{19}$ (23.1 mol % Ga_2O_3) is very close to the proposed phase of $Sr_7Ga_4O_{13}$. Possibly decastrontium hexagallate was misinterpreted as heptastrontium tetragallate. The same assumption was made in more recent work by Zinkevich (2007). However, we cannot exclude that both of them are stable phases. Including the results of this work, at least four polymorphs are known for $Sr_{10}Ga_6O_{19}$: α and β (Kahlenberg, 2002) as well as the superstructures reported here.

The authors are grateful to K. J. Webb for proof-reading the manuscript.

References

Batti, P. & Sloccari, G. (1969). *Ann. Chim. (Rome)*, **59**, 155–162.
Becker, P. J. & Coppens, P. (1974). *Acta Cryst.* A**30**, 129–147.
Brown, I. D. & Altermatt, D. (1985). *Acta Cryst.* B**41**, 244–247.
Finger, L. W., Kroeker, M. & Toby, B. H. (2007). *J. Appl. Cryst.* **40**, 188–192.
Janssen, T., Janner, A., Looijenga-Vos, A. & de Wolff, P. M. (2004). *International Tables for Crystallography*, Vol. C, ch. 9.8, 3rd ed. Dordrecht: Kluwer Academic Publishers.
Kahlenberg, V. (2001). *J. Solid State Chem.* **160**, 421–429.
Kahlenberg, V. (2002). *Solid State Sci.* **4**, 183–189.
Kahlenberg, V., Lazić, B. & Krivovichev, S. V. (2005). *J. Solid State Chem.* **178**, 1429–1439.
Kobzareva, V. P., Kovba, L. M., Lopato, L. M., Lykova, L. N. & Shevchenko, A. V. (1976). *Russ. J. Inorg. Chem.* **21**, 1651–1654.
Krüger, H. & Breil, L. (2009). *J. Appl. Cryst.* **42**, 140–142.
Palatinus, L. (2009). Personal communication.
Palatinus, L. & van Smaalen, S. (2002). *Acta Cryst.* A**58**, 559–567.
Palatinus, L. & van Smaalen, S. (2004). *Z. Kristallogr.* **219**, 719–729.
Petříček, V., Dušek, M. & Palatinus, L. (2000). *JANA*2000. Institute of Physics, Prague, Czech Republic.
Poort, S. H. M., Blokpoel, W. P. & Blasse, G. (1995). *Chem. Mater.* **7**, 1547–1551.
Sakata, M. & Sato, M. (1990). *Acta Cryst.* A**46**, 263–270.
Smaalen, S. van, Palatinus, L. & Schneider, M. (2003). *Acta Cryst.* A**59**, 459–469.
Stoe & Cie GmbH (2007). *X-Area 1.39*. Darmstadt, Germany.
Yang, S.-H. & Tu, H.-F. (2005). *J. Electrochem. Soc.* **152**, H1–H5.
Zinkevich, M. (2007). *Int. J. Mater. Res.* **98**, 574–579.